Magnetic flux conservation in an imploding plasma

F. García-Rubio, J. Sanz, and R. Betti

Phys. Rev. E **97**, 011201 — Published 8 January 2018

DOI: 10.1103/PhysRevE.97.011201

Magnetic Flux Conservation in an Imploding Plasma

F. García-Rubio
E.T.S.I. Aeronáutica y del Espacio, Universidad Politécnica de Madrid, Madrid 28040, Spain.

J. Sanz
E.T.S.I. Aeronutica y del Espacio, Universidad Politcnica de Madrid, Madrid 28040, Spain.

R. Betti
Laboratory for Laser Energetics, Department of Mechanical Engineering, and Physics and Astronomy, University of Rochester, New York 14623.
(Dated: December 18, 2017)

The theory of magnetic flux conservation is developed for a subsonic plasma implosion and used to describe the magnetic flux degradation in the MagLIF concept [S. A. Slutz *et al.* Phys. Plasmas 17, 056303 (2010)]. Depending on the initial magnetic Lewis and Péclet numbers and the electron Hall parameter, the implosion either falls into a superdiffusive regime in which the magnetization decreases or a magnetized regime in which the magnetization increases. Scaling laws for magnetic field, temperature and magnetic flux losses in the hot spot of radius R are obtained for both regimes. The Nernst velocity convects the magnetic field outwards, pushing it against the liner and enhancing the magnetic field diffusion, thereby reducing the magnetic field compression and degrading the implosion performance. However, in the magnetized regime, the core of the hot spot becomes magnetically insulated and undergoes an ideal adiabatic compression ($T \sim R^{-4/3}$ compared to $T \sim R^{-2/3}$ without magnetic field), while the detrimental Nernst term is confined to the outer part of the hot spot. Its effect is drastically reduced, improving the magnetic flux conservation.

In inertial confinement fusion (ICF), fuel areal densities $\rho R > 0.3$ g/cm^2 and implosion velocities exceeding 30 cm/μs are required for the onset of the ignition process[1]. Magneto inertial fusion (MIF) concepts[2, 3] are based on magnetizing the fuel in order to suppress heat losses and enhance confinement of the fusion products[4], thereby relaxing implosion velocity and areal density requirements and increasing fusion yields[5, 6].

In 2010, Slutz *et al.*[7] proposed the magnetized liner inertial fusion (MagLIF) scheme, in which a pulsed power device drives the implosion of a cylindrical beryllium liner filled with fusion fuel. The target is initially magnetized with a $10-30$T magnetic field, and the fuel is preheated by a laser to temperatures $200-400$ eV. The implosion velocity is of the order of 10 cm/μs, while the final areal density is about 0.07 g/cm^2. The first fully integrated experiments testing the MagLIF concept produced up to 2×10^{12} thermonuclear deuterium-deuterium neutrons, demonstrating its viability[8]. In 2012, Slutz and Vesey[9] reported implosions simulations of targets in which a dense cryogenic deuterium-tritium layer is added on the inside surface of the metal liner. The fusion energy gains exceeded 100, which is adequate for fusion energy applications.

A major degradation mechanism reported in Ref. 7 is the loss of magnetic flux during compression caused by the Nernst effect (magnetic field convection due to perpendicular temperature gradients), which degrades the fusion yield enhancement. Understanding the Nernst effect as well as the evolution of the magnetohydrodynamic variables is a crucial step to improve the design of this scheme. In MagLIF implosions, the Mach number Ma is typically less than unity. Subsonic unmagnetized implosions have been analytically studied in an ICF context[10–13], whereas the Nernst term effect on magnetic flux conservation in a plasma slab in contact with a cold wall has been investigated in Refs. 14 and 15.

In this work, we describe a detailed analytical model of a cylindrical subsonic magnetized plasma implosion, relevant for free fall, deceleration and stagnation phases. We consider a deuterium plasma (hot spot) surrounded by an imploding shell of cold high-density plasma (liner) made of the same material for simplicity. The independent variables are time t and radial distance r. We analyze the hot spot region limited by the inner wall of the liner, $r = R(t)$. The implosion velocity $V_i = -\mathrm{d}R/\mathrm{d}t$ is assumed to be constant and set by the conditions during the acceleration phase. We consider a fully ionized plasma fluid model with Braginskii's expressions and notation for the transport coefficients[16] and the ideal gas assumption with adiabatic index $\gamma = 5/3$. The state of the plasma is determined by the ion particle density n, plasma temperature T, pressure $p = p_i + p_e = 2nT$, radial velocity v and axial magnetic field B. We introduce the thermal to magnetic pressure ratio $\beta = 8\pi p_c/B_c^2$. Hereinafter, the sub-index c denotes the value of the variables at the center $r = 0$ (symmetrical axis), which evolve in time, while the sub-index 0 refers to the value at $t = 0$. The problem is greatly simplified noticing that $\mathrm{Ma} \ll 1$ and $\beta \gg 1$ in many typical implosions. The analysis is performed in this double limit. Momentum conservation simplifies to isobaricity $p(t, r) = p_c(t)$. Ion continuity, total energy conservation and induction equations read:

$$\frac{\partial n}{\partial t} + \frac{1}{r}\frac{\partial}{\partial r}\left(rvn\right) = 0, \tag{1}$$

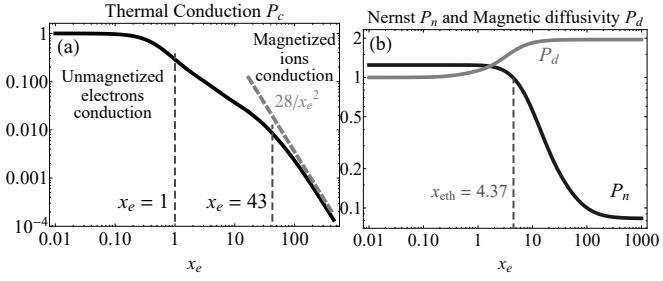

FIG. 1. Dependence of transport coefficients on the magnetization (electron Hall) parameter x_e.

$$v = -\frac{r}{2\gamma p_c}\frac{\mathrm{d}p_c}{\mathrm{d}t} + \frac{\gamma-1}{\gamma p_c}\chi_\perp \frac{\partial T}{\partial r}, \tag{2}$$

$$\frac{\partial B}{\partial t} + \frac{1}{r}\frac{\partial}{\partial r}(rvB) = \frac{1}{r}\frac{\partial}{\partial r}\left(r\underbrace{D_{m\perp}\frac{\partial B}{\partial r}}_{\text{Joule}} + r\underbrace{\frac{c\beta_\wedge^{uT}}{en}\frac{\partial T}{\partial r}}_{\text{Nernst}}\right). \tag{3}$$

The coefficient $\chi_\perp$ accounts for electron plus ion conductivities, $D_{m\perp} = \alpha_\perp c^2/4\pi e^2 n^2$ is the magnetic field diffusion coefficient appearing in the Joule term, and $\beta_\wedge^{uT}$ refers to the transport coefficient for the thermoelectric Nernst effect.

As initial conditions, we impose that the target is uniformly magnetized with an external magnetic field B_0. Additionally, an initial temperture profile needs to be proposed. As boundary conditions, we consider that during the implosion, the liner remains colder than the plasma in the hot spot: $T(R,t) = 0$. The cold dense liner acts as an electric insulator where currents cannot flow, and the axial magnetic field is equal to the external field, $B(R,t) = B_0$. In addition, we require $v = \mathrm{d}R/\mathrm{d}t$ $(= -V_i)$ at $r = R$. The thermal conductivity can be neglected at the inner liner surface, and the heat conduction losses are recycled back via the ablated liner material[10, 11] ($r = R$ represents an ablation front). The energy conservation balance in the hot spot enclosed by the cold liner states that, although the hot spot mass increases with time, it behaves like a closed system that is adiabatically heated: $p_c R^{2\gamma}$ is kept constant.

We normalize the spatial coordinate, $\eta = r/R(t)$, the implosion time, $\tau = \log[R_0/R(t)]$, the plasma temperature $\theta(\eta,\tau) = [T/T_c(\tau)]^{5/2}$, magnetic field $\phi(\eta,\tau) = B/B_c(\tau)$ and velocity $u(\eta,\tau) = v/V_i$. The transport coefficients can therefore be written as $\chi_\perp = \bar{K}T_c^{5/2}\theta\mathcal{P}_c$, $D_{m\perp} = \bar{D}T_c^{-3/2}\theta^{-3/5}\mathcal{P}_d$, with $\bar{K} = 8.64\times 10^{27}$ sec^{-1}cm^{-1}keV$^{-5/2}$ and $\bar{D} = 93.2$ cm^{2}keV$^{3/2}$/sec conductivity and diffusivity constants, and $c\beta_\wedge^{uT}/en = [(\gamma-1)\chi_\perp/\gamma p]\mathcal{P}_n B$. The latter relation indicates that the Nernst term in Eq. 3 accounts for magnetic field convection in the heat flux direction. The terms $\mathcal{P}_c(x_e)$, $\mathcal{P}_n(x_e)$ and $\mathcal{P}_d(x_e)$ represent the effect of magnetization on thermal conduction, Nernst effect and magnetic diffusivity, respectively[14]. They are rational functions of the local electron Hall parameter (electron cyclotron frequency times the electron collision time) $x_e = \omega_e\tau_e = x_{ec}\theta\phi$ and plotted in Fig. 1:

$$\mathcal{P}_c(x_e) = \frac{\gamma_1' x_e^2 + \gamma_0'}{\gamma_0\Delta_e} + \sqrt{\frac{2m_e}{m_i}}\frac{2x_i^2 + 2.645}{\gamma_0\Delta_i},$$

$$\mathcal{P}_n(x_e) = \frac{2\gamma}{\gamma-1}\frac{\beta_1'' x_e^2 + \beta_0''}{\gamma_1' x_e^2 + \gamma_0' + \sqrt{\frac{2m_e}{m_i}}\frac{\Delta_e}{\Delta_i}(2x_i^2 + 2.645)},$$

$$\mathcal{P}_d(x_e) = \frac{1 - \dfrac{\alpha_1' x_e^2 + \alpha_0'}{\Delta_e}}{\alpha_0},$$

with $\Delta_e = x_e^4 + \delta_1 x_e^2 + \delta_0$ and $\Delta_i = x_i^4 + 2.70x_i^2 + 0.677$, and $x_i = \omega_i\tau_i = \sqrt{2m_e/m_i}x_e$ standing for the ion magnetization. The values for the coefficients γ_0', δ_0, etc are taken from Braginskii[16] and specified for a deuterium plasma ($Z = 1$, $A = 2$). A blow-off velocity based on thermal conduction can be defined as $V_b = 2(\gamma-1)\bar{K}T_c^{7/2}/5\gamma R p_c$[10–13]. The global plasma parameters are thereby reduced to three dimensionless numbers: the Péclet number $\mathrm{Pe} = V_i/V_b$, the magnetic Reynolds number $\mathrm{Re} = V_i R/D_c$, with $D_c = \bar{D}T_c^{-3/2}$, and the electron Hall parameter at the center x_{ec}. These numbers evolve during the implosion. For convenience, we use the magnetic Lewis number instead of the Reynolds, defined as $\mathrm{Le} = V_b R/D_c = \mathrm{Re}/\mathrm{Pe}$. In addition, the thermal to magnetic pressure ratio β can be related to Le, x_{ec} through:

$$\mathrm{Le} = \frac{(\gamma-1)\gamma_0}{20\gamma\alpha_0}\beta x_{ec}^2 = 0.12\beta x_{ec}^2. \tag{4}$$

In order to be consistent with the $\beta \gg 1$ assumption, we restrict our analysis to $\mathrm{Le} \gg x_{ec}^2$.

The dimensionless velocity can be written as $u = -\eta + u_c$, where $u_c = (1/\mathrm{Pe})\mathcal{P}_c\theta^{2/5}\partial\theta/\partial\eta$ stands for the contribution of thermal conduction. Using this expression, Eqs. (1), (3) after normalization read:

$$\frac{\partial\theta^{2/5}}{\partial\tau} - \lambda_T\theta^{2/5} = \frac{\theta^{4/5}}{\mathrm{Pe}\eta}\frac{\partial}{\partial\eta}\left(\eta\mathcal{P}_c\frac{\partial\theta}{\partial\eta}\right), \tag{5}$$

$$\frac{\partial\phi}{\partial\tau}-\lambda_B\phi+\frac{1}{\mathrm{Pe}\eta}\frac{\partial}{\partial\eta}\left[\eta\mathcal{P}_c\left(1-\mathcal{P}_n\right)\theta^{2/5}\frac{\partial\theta}{\partial\eta}\phi\right]=\frac{1}{\mathrm{PeLe}\eta}\frac{\partial}{\partial\eta}\left(\eta\mathcal{P}_d\theta^{-3/5}\frac{\partial\phi}{\partial\eta}\right), \tag{6}$$

where the eigenvalues $\lambda_T = \left(\mathrm{d}n_c/\mathrm{d}\tau\right)/n_c - 2 = 2(\gamma - 1) - \left(\mathrm{d}T_c/\mathrm{d}\tau\right)/T_c$ and $\lambda_B = 2 - \left(\mathrm{d}B_c/\mathrm{d}\tau\right)/B_c$, with $n_c = p_c/2T_c$, describe the evolution of the variables at the center and measure how much it differs from an ideal implosion (infinite Pe and Re: no ablation and $n_c \sim R^{-2}$, $T_c \sim R^{-4/3}$, $B_c \sim R^{-2}$). Two opposite effects are accounted for in the advection term in Eq. (6): convection due to u_c, in the opposite direction to the heat flux, and convection due to the Nernst term, in the same direction. For $x_e < x_{e\mathrm{th}} = 4.37$, $1-\mathcal{P}_n$ is negative and the latter prevails, Fig. 1(b). All the information about the initial state is condensed into the initial Péclet Pe_0 and Lewis Le_0 numbers, the initial Hall parameter x_{ec0} and the initial profiles for θ and ϕ.

The system (5)-(6) is coupled through the magnetization effect on the thermal conductivity, $\mathcal{P}_c(x_e)$. Solving it allows to obtain the temperature and magnetic field profiles and the eigenvalues λ_T and λ_B. From the definition of Pe, Le and x_{ec}, their evolution in time can be easily described in terms of λ_T and λ_B:

$$\frac{\mathrm{d}\log\mathrm{Pe}}{\mathrm{d}\tau}=\frac{7}{2}\left(\lambda_T-\frac{2}{3}\right), \tag{7}$$

$$\frac{\mathrm{d}}{\mathrm{d}\tau}\left(\mathrm{LePe}^{10/7}\right)=0, \tag{8}$$

$$\frac{\mathrm{d}\log x_{ec}}{\mathrm{d}\tau}=2-\lambda_B-\frac{5}{2}\lambda_T. \tag{9}$$

In order to gain insight into the physics of the implosion, we first consider the case where the magnetization is very low $x_{ec} \ll 1$. In this limit, $\mathcal{P}_c = 1$, Eq. (5) is decoupled from (6), and simplifies to:

$$\frac{\partial\theta^{2/5}}{\partial\tau}-\lambda_T\theta^{2/5}=\frac{\theta^{4/5}}{\mathrm{Pe}\eta}\frac{\partial}{\partial\eta}\left(\eta\frac{\partial\theta}{\partial\eta}\right). \tag{10}$$

This equation has a stable stationary solution $\theta_s(\eta)$[10–13], corresponding to a self-similar implosion, Fig. 2(a). In this self-similar state, $\mathrm{Pe}\lambda_T = 3.48$, and inserting this into Eq. (7), we obtain that the Péclet number tends to a constant $\mathrm{Pe} = \mathrm{Pe}_s = 5.22$, and $\lambda_T = 2/3$. Consequently, the Lewis number also tends to a constant whose value depends upon the initial conditions: $\mathrm{Le} = \mathrm{Le}_0\left(\mathrm{Pe}_0/\mathrm{Pe}_s\right)^{10/7}$. The velocity self-similar profile is $u_s(\eta) = -\eta + \left(1/\mathrm{Pe}_s\right)\theta_s^{2/5}\mathrm{d}\theta_s/\mathrm{d}\eta$. The temperature at the center evolves as $T_c \sim R^{-2/3}$, while the hot spot mass $M_h = 2\pi\int_{r=0}^{r=R} nr\mathrm{d}r$ increases as $M_h \sim R^{-2/3}$. Material from the cold liner is ablated into the hot spot, cooling it down and causing the temperature increase to be less than expected for an ideal adiabatic compression of a gas $\left(T \sim R^{-4/3}\right)$.

In the unmagnetized limit ($x_{ec} \ll 1$), Eq. (6) simplifies to:

$$\frac{\partial\phi}{\partial\tau}-\lambda_B\phi+\frac{\delta}{\mathrm{Pe}\eta}\frac{\partial}{\partial\eta}\left(\eta\theta^{2/5}\frac{\partial\theta}{\partial\eta}\phi\right)=\frac{1}{\mathrm{PeLe}\eta}\frac{\partial}{\partial\eta}\left(\eta\theta^{-3/5}\frac{\partial\phi}{\partial\eta}\right), \tag{11}$$

where the parameter $\delta = 1 - \mathcal{P}_n(0) = -0.24$ can be switched to $\delta = 1$ in order to artificially turn the Nernst term off for comparison purposes. Once the temperature reaches the self-similar state, the magnetic field also tends to a stationary self-similar solution $\phi = \phi_s(\eta;\mathrm{Le})$, and $\lambda_B = \lambda_B(\mathrm{Le})$ gets independent of time. The magnetic field at the center evolves as $B_c \sim R^{\lambda_B - 2}$, whereas the magnetic flux $\Phi = 2\pi\int_{r=0}^{r=R} Br\mathrm{d}r$ decreases as $\Phi \sim R^{\lambda_B}$. The eigenvalue λ_B and the self-similar profile ϕ_s are shown in Figs. 2(b), 2(c), 2(d) as a function of the Lewis number.

When the Lewis number is small, the parameter $\lambda_B = 2$, the magnetic field at the center B_c attains a constant value and consequently the magnetic flux decreases as $\Phi \sim R^2$. However, for $\mathrm{Le} > 0.93$ with Nernst and $\mathrm{Le} > 0.78$ without, $\lambda_B < 2$ and the magnetic field at the center increases in time.

When the Lewis number is large, diffusion can be neglected in principle and the magnetic field is convected by the plasma motion and the Nernst velocity. If the latter is not taken into account, the magnetic field is frozen into the plasma and the mass ablated into the hot spot would squeeze it inwards, steepening the B-field profile until diffusion becomes important. An asymptotic analysis in this large Lewis number and no Nernst limit shows that the self-similar profile is $\phi_s(\eta) = \exp\left(-\mathrm{Pe}_s\mathrm{Le}\eta^2/6\right)$, the field is not diffused through the liner, $\lambda_B \to 0$ and the magnetic flux is conserved. When the Nernst term is taken into account, the Nernst convection dominates and the magnetic field is advected outwards. It penetrates into the ablated mass, it is pushed against the liner and dissipated in a thin layer where diffusion becomes important. An asymptotic expansion for large Lewis numbers shows that the thickness of the diffusion layer is $O\left(1/\sqrt{\mathrm{Le}}\right)$ and the peak of the profile scales as $\mathrm{Le}^{1/5}$. The parameter $\lambda_B \to -2\delta/3 \approx 0.16$, and cannot be further reduced by increasing the Lewis number, which indicates that the Nernst term plays a crucial role in degrading the magnetic flux conservation during the implosion even for a very conductive plasma.

According to Faraday-Lenz's law, the magnetic field in the hot spot is always compressed. The evolution of

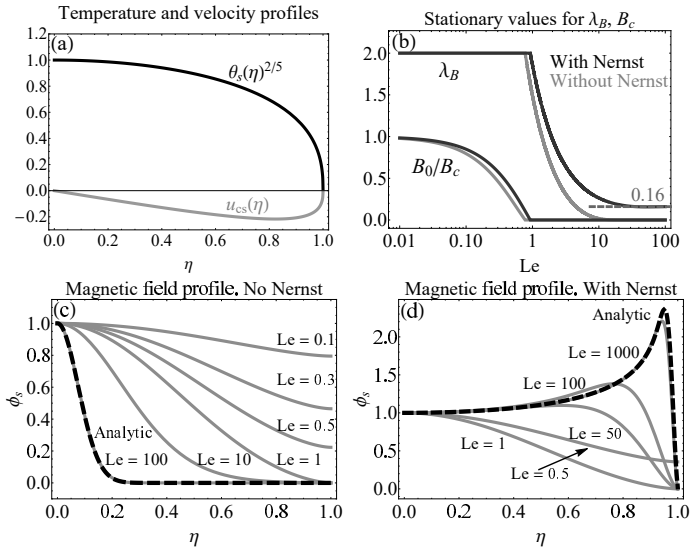

FIG. 2. Unmagnetized plasma implosion. (a) Temperature and velocity self-similar profiles. (b) Stationary values for λ_B and B_c. (c), (d) Magnetic field self-similar profiles.

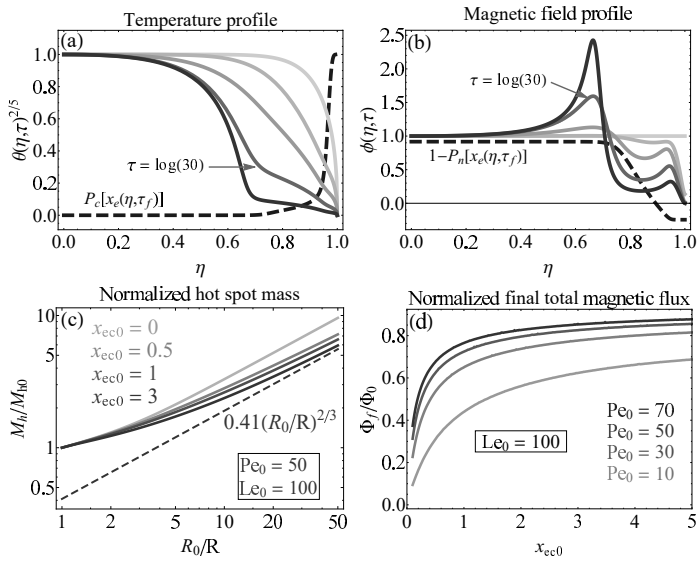

FIG. 3. (a), (b) Magnetized implosion profiles. Initial parameters: $Pe_0 = 50$, $Le_0 = 100$, $x_{ec0} = 1.5$, $\theta_0(\eta) = \cos\left(\pi\eta^6/2\right)$, $\phi_0(\eta) = 1$. From light to darker gray: $\tau = 0,\ 1,\ 2,\ \tau_f = \log(30) \approx 3.4,\ 5$. (c) Normalized hot spot mass in implosions with the same initial parameters but different initial magnetization. (d) Normalized final magnetic flux remaining in the hot spot in implosions with different initial magnetization.

the magnetization depends, however, on a balance between the collision and cyclotron frequencies, Eq. (9). In the low magnetization limit ($\omega_e\tau_e < 1, \lambda_T = 2/3$), the collision frequency increases more than the cyclotron frequency whenever $\lambda_B < 1/3$, hence the magnetization decreases in time and the hot spot remains unmagnetized during the whole implosion. This unmagnetized regime represents an attractor of the complete system of equations (5)-(6), and will be denoted as "superdiffusive regime". For $\lambda_B > 1/3$, which takes place for $\mathrm{Le} > \mathrm{Le}_{cr} = 7.10$ with Nernst and $\mathrm{Le} > 3.02$ without, the collision frequency increases less than the cyclotron frequency, the hot spot gets magnetized and the hydrodynamic profiles are consequently modified.

We consider now a strong magnetization limit, $x_{ec} \gg 1$. The plasma is magnetically insulated at the center, and the continuity and induction equations (5), (6) give $\lambda_T = 0$, $\lambda_B = 0$. The central temperature and magnetic field undergo an ideal adiabatic compression: $T_c \sim R^{-4/3}$, $B_c \sim R^{-2}$. The Péclet number evolves as $\mathrm{Pe} \sim R^{7/3}$, and consequently $\mathrm{Le} \sim R^{-10/3}$. In this limit, Eq. (9) establishes that the magnetization keeps increasing in time as $x_{ec} \sim R^{-2}$, hence this regime represents another attractor, which will be denoted as "magnetized regime". According to Eq. (4), the pressure ratio β decreases in this limit as $\beta \sim R^{2/3}$. Therefore, pressure ratios of order unity and below could be attained by the end of the implosion. Consequently, for these results to be valid in the magnetized regime for a suffciently long time, β has to be large initially, which is typically the case in MagLIF ($\beta_0 \sim$ several hundred).

In Figs. 3(a) and (b), the temporal evolution of the temperature and magnetic field profiles of a magnetized implosion are shown. The initial state corresponds to a characteristic MagLIF parameter range: $\mathrm{Pe}_0 = 50$, $\mathrm{Le}_0 = 100$ and $x_{ec0} = 1.5$, which gives $\beta_0 = 361$, and we choose $\theta_0(\eta) = \cos\left(\pi\eta^6/2\right)$, $\phi_0(\eta) = 1$. In this case study, the magnetization increases in time and the magnetized regime is reached. The temperature profile presents two distinguishable regions. Close to the liner, where the temperature is low and the plasma is unmagnetized, cold material is ablated through the ablation front. It penetrates into the hot spot until it reaches the magnetically insulated region, where $\mathcal{P}_c \approx 0$ and $u_c \approx 0$. More and more layers of cold material are accumulated at the outer part of the hot spot, cooling it down and forming an ablation front like structure that separates the hot highly magnetized plasma from the cold less magnetized plasma.

The Nernst term is confined within the unmagnetized region. Close to the liner, where $1 - \mathcal{P}_n < 0$, the magnetic field is pushed towards it and dissipated in a thin layer. Deeper into the hot spot, the Nernst term is drastically reduced, and the advection direction is inverted: $1 - \mathcal{P}_n > 0$. The magnetic field is convected by the plasma motion inwards and accumulates at the border of the highly magnetized region. Consequently, the magnetic field in the less magnetized region is expelled out both to the liner and to the hot plasma. The magnetic field dissipated at the liner cannot thereby be replaced and the normalized B-field in the cold region decreases. During this process, the width of the diffusion layer is maintained, but the magnetic field peak is reduced until the layer eventually vanishes and the magnetic flux losses are thereon suppressed.

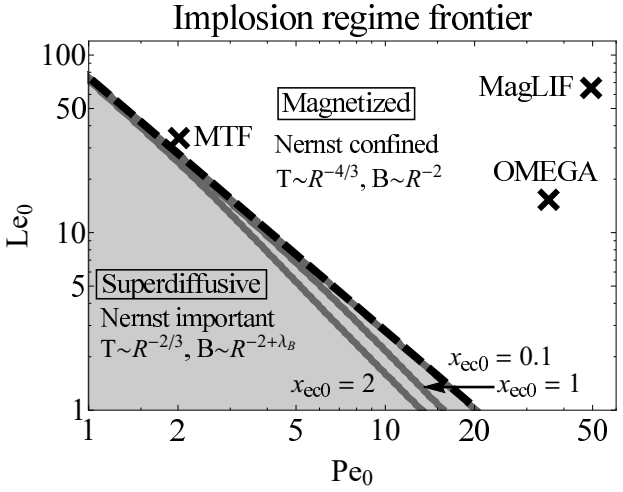

FIG. 4. Parameter frontier for superdiffusive and magnetized implosion regimes. The dashed line corresponds to $\mathrm{Le}_0\mathrm{Pe}_0^{10/7} = 75$. The crosses indicate the position in the chart of the three schemes in Table I.

The magnetization decreases mass ablation and improves magnetic flux conservation. In the magnetized regime, the hot spot mass also scales asymptotically as $M_h \sim R^{-2/3}$, but the constant of proportionality is reduced, Fig. 3(c). As previously commented, the diffusion layer tends to vanish in this limit, the magnetic flux losses are drastically reduced and the magnetic flux in the hot spot reaches a constant value Φ_f dependent upon the initial state, shown in Fig. 3(d).

Whether an implosion falls into the superdiffusive or magnetized regime depends on the initial Péclet, Lewis and Hall parameter. In Fig. 4, the boundary between both regimes is plotted in a $\mathrm{Pe}_0 - \mathrm{Le}_0$ map for different x_{ec0}. For a small initial magnetization, the border corresponds to $\mathrm{Le}_0\mathrm{Pe}_0^{10/7} = \mathrm{Le}_{cr}\mathrm{Pe}_s^{10/7} \approx 75$, which falls back to lower values of Le_0, Pe_0 when the initial magnetization is increased.

According to the results previously derived, in the design of magnetized inertial fusion implosions it is important to be placed in the "Magnetized regime" part of the chart plotted in Fig. 4. This can be assured if the implosion design point satisfies

$$\mathrm{Le}_0\mathrm{Pe}_0^{10/7} = 386 \left(\frac{T_0}{1\ \mathrm{eV}}\right)^{3/7} \left(\frac{\rho_0}{1\ \mathrm{mg/cm^3}}\right)^{3/7} \left(\frac{R_0}{1\ \mathrm{cm}}\right)^{10/7} \left(\frac{V_i}{1\ \mathrm{cm}/\mu\mathrm{s}}\right)^{10/7} > 75, \quad (12)$$

where R_0 and ρ_0 are the initial radius and fuel density. In Table I, three different schemes have been analyzed, and their position is shown in Fig. 4. Both the pulsed power MagLIF and laser driven magnetized liner implosions tested at Laboratory for Laser Energetics satisfy well this requirement, but the low density, low implosion velocity regime explored in the past by Lindemuth and Kirkpatrick[2] in spherical geometry may need to be adjusted for cylindrical geometry since it lays close to the threshold.

	MagLIF	OMEGA	MTF
T_0(eV)	300	200	50
ρ_0(mg/cm^3)	3	2.7	0.005
R_0(cm)	0.2	.03	0.5
V_i(cm/μs)	10	18.8	1
Pe_0	53	37	2
Le_0	67	15	31
$\mathrm{Le}_0\mathrm{Pe}_0^{10/7}$	20.000	2.500	80

TABLE I. Characteristic initial values of the magnethydrodynamic variables for three different magnetized inertial fusion schemes. MagLIF corresponds to Ref. 7, OMEGA corresponds to the laser-driven magnetized liner inertial fusion studied at the LLE (OMEGA Laser) in Refs. 17 and 18, and MTF corresponds to the magnetized target fusion regime explored in spherical geometry in Ref. 2.

To conclude, the existence of two regimes, superdiffusive and magnetized, has been proved in a hot spot model of magnetized cylindrical implosions. Scaling laws for temperature, magnetic field, mass ablation and magnetic flux losses for every regime have been derived. The Nernst term convects the magnetic field outwards and enhances diffusion, degrading thereby the magnetic flux conservation even for a highly conductive plasma. In the magnetized regime, the core of the hot spot gets magnetically insulated, and the effect of the Nernst term is reduced since it is confined to the outer part of the hotspot close to the liner.

This research was supported by the Spanish Ministerio de Economa y Competitividad, Project No. ENE2014-54960R, the Spanish Ministerio de Educacin, Cultura y Deporte under the national research program FPU, grant FPU 14/04879 and the U.S. Department of Energy, awards DE-SC0016258 and DE-AR0000568.

[1] S. Atzeni and J. Meyer-ter Vehn, *The Physics of Inertial Fusion: BeamPlasma Interaction, Hydrodynamics, Hot Dense Matter*, 125 (Oxford University Press on Demand, 2004).

[2] I. R. Lindemuth and R. C. Kirkpatrick, Nucl. Fusion **23**, 263 (1983).
[3] R. C. Kirkpatrick, I. R. Lindemuth, and M. S. Ward, Fusion Technol. **27**, 201 (1995).
[4] M. M. Basko, A. J. Kemp, and J. Meyer-ter Vehn, Nucl. Fusion **40**, 59 (2000).
[5] P. Y. Chang, G. Fiksel, M. Hohenberger, J. P. Knauer, R. Betti, F. J. Marshall, D. D. Meyerhofer, F. H. Séguin, and R. D. Petrasso, Phys. Rev Lett. **107**, 035006 (2011).
[6] M. Hohenberger, P. Y. Chang, G. Fiksel, J. P. Knauer, R. Betti, F. J. Marshall, D. D. Meyerhofer, F. H. Séguin, and R. D. Petrasso, Phys. Plasmas **19**, 056306 (2012).
[7] S. A. Slutz, M. C. Herrmann, R. A. Vesey, A. B. Sefkow, D. B. Sinars, D. C. Rovang, K. J. Peterson, and M. E. Cuneo, Phys. Plasmas **17**, 056303 (2010).
[8] M. R. Gomez, S. A. Slutz, A. B. Sefkow, D. B. Sinars, K. D. Hahn, S. B. Hansen, E. C. Harding, P. F. Knapp, P. F. Schmit, C. A. Jennings, *et al.*, Phys. Rev. Lett. **113**, 155003 (2014).
[9] S. A. Slutz and R. A. Vesey, Phys. Rev. Lett. **108**, 025003 (2012).
[10] R. Betti, M. Umansky, V. Lobatchev, V. N. Goncharov, and R. L. McCrory, Phys. Plasmas **8**, 5257 (2001).
[11] J. Sanz and R. Betti, Phys. Plasmas **12**, 042704 (2005).
[12] J. Sanz, J. Garnier, C. Cherfils, B. Canaud, L. Masse, and M. Temporal, Phys. Plasmas **12**, 112702 (2005).
[13] J. Garnier and C. Cherfils, Phys. Plasmas **12**, 012704 (2005).
[14] F. García-Rubio and J. Sanz, Phys. Plasmas **24**, 072710 (2017).
[15] A. L. Velikovich, J. L. Giuliani, and S. T. Zalesak, Phys. Plasmas **22**, 042702 (2015).
[16] S. I. Braginskii, Reviews of Plasma Physics **1**, 205 (1965).
[17] J. R. Davies, D. H. Barnak, R. Betti, E. M. Campbell, P.-Y. Chang, A. B. Sefkow, K. J. Peterson, D. B. Sinars, and M. R. Weis, Phys. Plasmas **24**, 062701 (2017).
[18] D. H. Barnak, J. R. Davies, R. Betti, M. J. Bonino, E. M. Campbell, V. Y. Glebov, D. R. Harding, J. P. Knauer, S. P. Regan, A. B. Sefkow, *et al.*, Physics of Plasmas **24**, 056310 (2017).